

# Anthropogenic land consolidation intensifies zoonotic host diversity loss and disease transmission in human habitats

Received: 6 February 2024

Accepted: 30 September 2024

Published online: 18 November 2024

 Check for updates

Shan Pei <sup>1,2,17</sup>, Pengbo Yu ✉<sup>3,17</sup>, Jayna Raghwani<sup>4,17</sup>, Yuxin Wang<sup>2</sup>, Ziyang Liu<sup>1</sup>, Yidan Li<sup>1</sup>, Yanchao Cheng<sup>1</sup>, Qiushi Lin<sup>1</sup>, Chuliang Song <sup>5</sup>, Guha Dharmarajan<sup>6</sup>, Christina L. Faust <sup>7</sup>, Yunyu Tian <sup>1</sup>, Yiting Xu<sup>1</sup>, Yilin Liang<sup>1</sup>, Jianhui Qu<sup>3</sup>, Jing Wei<sup>3</sup>, Shen Li<sup>3</sup>, Tongjun Zhang<sup>3</sup>, Chaofeng Ma <sup>8</sup>, Nita Bharti <sup>9</sup>, Bernard Cazelles <sup>10,11</sup>, Ruifu Yang <sup>12,18</sup>, Oliver G. Pybus <sup>4,13,18</sup>, Andrew P. Dobson <sup>5,18</sup>, Nils Chr. Stenseth <sup>14,15,16,18</sup>✉ & Huaiyu Tian <sup>1,18</sup>✉

Anthropogenic land-use change is an important driver of global biodiversity loss and threatens public health through biological interactions.

Understanding these landscape–ecological effects at local scales will help achieve the United Nations Sustainable Development Goals by balancing urbanization, biodiversity and the spread of infectious diseases. Here, we address this knowledge gap by analysing a 43-year-long monthly dataset (1980–2022) of synanthropic rodents in Central China during intensive land-use change. We observed a notable increase in the mean patch size, coinciding with a substantial change in rodent community composition and a marked decline in rodent diversity; eight of the nine local rodent species experienced near-extirpation. Our analysis reveals that these irregular species replacements can be attributed to the effect of land consolidation on species competition among rodents, favouring striped field mice, a critical reservoir host of Hantaan virus (HTNV). Consequently, land consolidation has facilitated the proliferation of striped field mice and increased the prevalence of HTNV among them. This study highlights the importance of considering both direct and indirect effects of anthropogenic activities in the management of biodiversity and public health.

Anthropogenic land-use change<sup>1</sup>, such as the conversion of natural habitats to agricultural or urban land, is an inevitable consequence of developing adequate and sustainable cities, one of the sustainable development goals (SDGs) proposed by the United Nations<sup>2–4</sup>. However, the conversion of landscapes has reshaped natural animal populations and their community structures<sup>5–8</sup>. Importantly, such disturbances do not affect all species equally but instead favour animals with generalist lifestyles, small body sizes and short generation times<sup>9–11</sup>. The increased tolerance of generalists to human-mediated disturbance is

evident in plants<sup>12</sup>, invertebrates<sup>13,14</sup>, birds<sup>15–19</sup> and mammals<sup>20,21</sup>. This pattern of differential species survival in anthropogenic environments has led to biotic homogenization around the world<sup>22–28</sup>. In addition, land conversion is also recognized as one of the major drivers of biodiversity loss, with species disappearing one-hundred times faster than in the prehuman period<sup>29,30</sup>. This is in contradiction with another SDG, that of halting biodiversity loss<sup>31–34</sup>. In this work, we demonstrate how anthropogenic land-use change impacts public health through its effects on zoonotic risks.

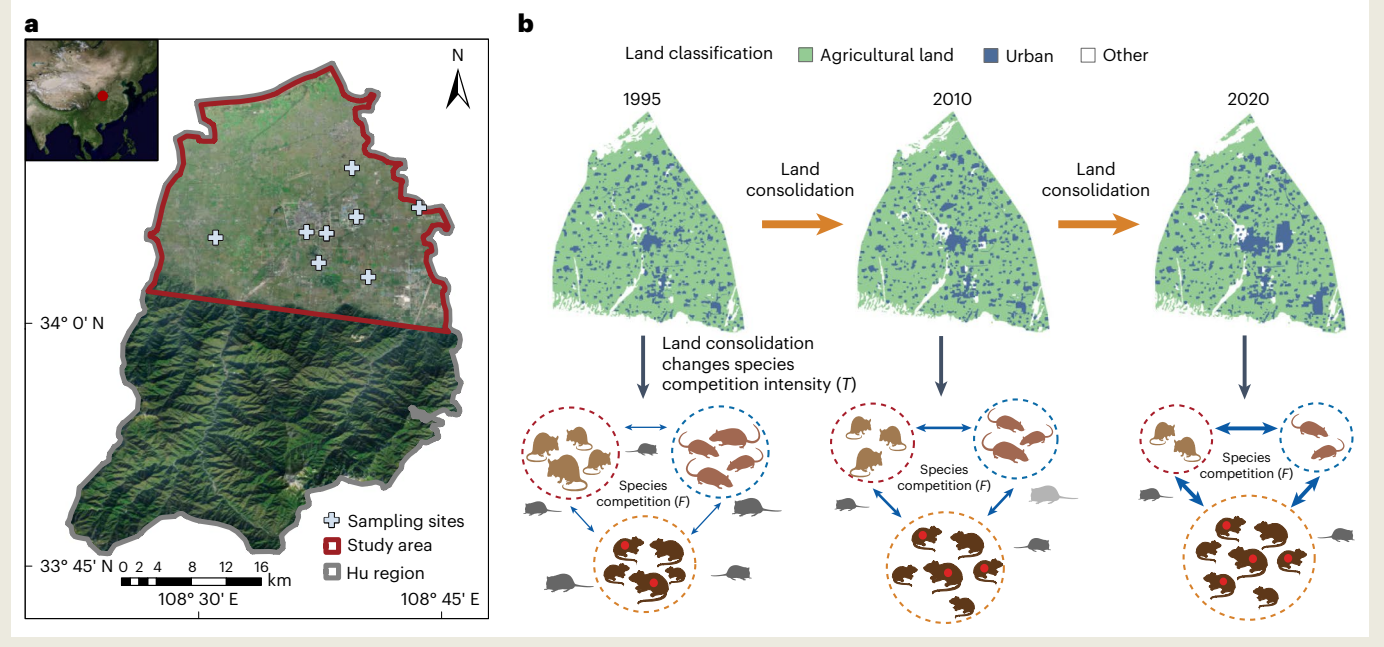
A full list of affiliations appears at the end of the paper. ✉ e-mail: [sxcdcy@126.com](mailto:sxcdcy@126.com); [n.c.stenseth@ibv.uio.no](mailto:n.c.stenseth@ibv.uio.no); [tianhuaiyu@gmail.com](mailto:tianhuaiyu@gmail.com)

## BOX 1

# Study area, anthropogenic land consolidation process and conceptual framework illustrating the potential consequences of land consolidation for public health and zoonosis risks

**a**, Study area, Hu region, China. **b**, Land consolidation process and potential consequences for public health and zoonosis risks. Land consolidation is the process of merging numerous heterogeneous small land parcels into larger homogeneous units. Spatial homogeneity may affect species competition among synanthropic rodents and decrease rodent diversity; such changes in the rodent community may, in turn, increase the risk of zoonotic diseases. Species competition involves intraspecific competition and interspecific competition. Rodent species include three numerically dominant rodents such as striped field mouse (*A. agrarius*, AA), Norway rat (*R. norvegicus*, RN) and buff-breasted rat (*R. flavipectus*, RF); as well as six other species such as rat-like hamster (*Cricetulus triton*), house mouse (*Mus musculus*), black rat (*Rattus rattus*), Chinese white-bellied rat

(*Niviventer confucianus*), harvest mouse (*Micromys minutus*) and an unknown species. Circles indicate the three most abundant rodent species: striped field mouse (dark brown), Norway rat (light brown) and buff-breasted rat (brown). Grey rodent symbols represent six other rodent species. Red dots indicate rodents carrying the HTNV. Black arrows illustrate the effect of land consolidation on species competition, while blue arrows correspond to interspecific competition. CCM is applied to initially explore the possible causal relationships between rodent species and the DLNM is used to investigate the potential nonlinear association between land consolidation and rodent population. On the basis of the analysis results, a multispecies population dynamic model is constructed, incorporating mean patch size, species competition and the rodent population growth rate.



Anthropogenic land-use change is usually associated with both loss of natural habitat (that is, habitat loss), as well as the alteration in the spatial configuration of habitat patches, also known as habitat fragmentation<sup>35,36</sup>. To reduce habitat fragmentation, China's policies and practices have advocated land consolidation<sup>37</sup>—the merging of many heterogeneous and small land patches into larger homogenous units. Over the last 40 years, China has undergone land conversion at an unprecedented rate, primarily as a result of urbanization (from 1978 onwards) and agricultural intensification (from 1986 onwards)<sup>38</sup>. Reducing fragmentation of parcels can improve infrastructure, enhance rural sustainable development and benefit ecosystem functioning (for example, soil structure<sup>39</sup>). However, despite reducing fragmentation, land consolidation can lead to notable changes in animal population dynamics and also negatively impact biodiversity through intensified agricultural practices and net loss of native habitat areas<sup>40–42</sup>.

Furthermore, land-use conversion and consolidation have rarely been directly linked to natural animal population dynamics and biodiversity on a regional scale over periods longer than a decade<sup>43</sup>. It is not clear how land consolidation affects synanthropic species, which may benefit from increased connectivity in human-modified habitats. In this study, our objective was to fill the knowledge gap by analysing a unique long-term dataset (1980–2022) collected from the Hu region of Central China. The Hu region has experienced intensive anthropogenic land-use change over the past four decades, where the rodent community consisted entirely of synanthropic species during the study period. Importantly, among those synanthropic rodents, the striped field mouse (*Apodemus agrarius*) is the local host of a zoonotic disease—Hantaan virus (HTNV) causing haemorrhagic fever with renal syndrome (HFRS)—and its population fluctuations are closely linked to HFRS incidence in human populations<sup>44,45</sup>. As a consequence, the Hu dataset is ideal for studying the long-term ecological responses of

synanthropic rodents to anthropogenic land-use change on a regional scale and understanding how changes in the rodent community contribute to zoonotic hazards.

We propose a conceptual framework of the interactions between anthropogenic land consolidation, synanthropic rodent community and public health (Box 1). Using this framework and with the aid of the Hu dataset, we explore how anthropogenic land consolidation affects the synanthropic rodent community and potentially further influences public health. We highlight the importance of long-term monitoring of wildlife in a human-mediated environment. Our findings suggest that anthropogenic disturbance not only affects human well-being directly by promoting improved infrastructure but also influences wildlife reservoirs of zoonotic pathogens.

## Results

### Observed dynamics in rodent diversity, community composition and HTNV prevalence

To measure the size and diversity of the rodent community, during the last four decades, >15,000 rodents of nine species were trapped in the Hu region, comprising >300,000 trap nights in total, with a mean capture rate of 4.88 rodents per 100 trap nights (range 0.33–15.21 per 100 trap nights). The abundance and composition of the rodent community changed strikingly in the Hu region (Fig. 1a). Although the abundances of most rodents decreased in the last four decades, the abundance of the striped field mouse increased, becoming the most abundant species in the community. We calculated species diversity on the basis of the effective number<sup>46,47</sup> of rodent species during this period (Fig. 1b) and found that diversity has decreased by 53% from 2.59 during 1980–1985 to 1.21 during 2017–2022. This represents a considerable decline in rodent diversity, with eight out of nine rodent species becoming nearly extinct in the Hu region over the 43 years of the study. These findings were quantitatively consistent with other measures of species diversity (Supplementary Fig. 1).

Land consolidation is an important consequence of the urbanization process in China<sup>48</sup>. By using high-resolution (30 m) land-use data (available from Landsat-MSS (1980) and Landsat-TM/ETM (1990–2022)), we detected strong temporal trends of land consolidation in the Hu region (Supplementary Fig. 2). This consolidation process contributed to a notable change in land-use configuration and reduction in heterogeneity. For both agricultural and urban land-use types, the number of patches has decreased substantially from 772 patches in 1980 to 404 in 2022, while the mean patch size has nearly tripled from 10.10 ha in 1980 to 28.04 ha in 2022 (Supplementary Fig. 2). Furthermore, we found a strong negative correlation between local rodent diversity and the mean patch size of anthropogenic habitats (rodent species diversity, Spearman's rank correlation coefficient  $\rho = -0.72$ ,  $P < 0.001$ ; species richness,  $\rho = -0.74$ ,  $P < 0.001$ ; Fig. 1b) and the distance between patches (rodent species diversity,  $\rho = -0.71$ ,  $P < 0.001$ ; species richness,  $\rho = -0.76$ ,  $P < 0.001$ ; Supplementary Fig. 3b), as well as a positive correlation between rodent diversity and edge density (rodent species diversity,  $\rho = 0.62$ ,  $P < 0.001$ ; and species richness,  $\rho = 0.72$ ,  $P < 0.001$ ; Supplementary Fig. 3c), indicating that rodent biodiversity loss in the Hu region was associated with a decrease in regional landscape heterogeneity. In particular, land consolidation was a monotonic process in the Hu region, while rodent species diversity decreased with population variations (Supplementary Figs. 1 and 2). The diagnostic results from the multiple regression revealed a high degree of correlation and collinearity among mean patch size, the distance between patches and edge density (Supplementary Table 1). Therefore, mean patch size was used as a proxy for land consolidation for subsequent analyses.

As the striped field mouse is the main reservoir host for HTNV, with infected individuals accounting for >95% of all infected rodents in the study area, we further investigated the prevalence of HTNV in this population over time (Fig. 1c). For striped field mice, we estimated the prevalence of HTNV from the accumulated number of

HTNV-positive individuals and the total number of trapped individuals per year. The prevalence of HTNV among striped field mice was positively correlated with the percentage of striped field mice comprising the rodent community (Fig. 1c;  $\rho = 0.41$ ,  $P < 0.01$ ). We also examined these associations using structural equation modelling (SEM)<sup>49</sup> within a single model framework. The results are consistent with our findings, indicating a direct positive effect of the percentage of striped field mice comprising the rodent community on the prevalence of HTNV, as well as the positive effect of land consolidation on the striped field mice in the rodent community (Supplementary Fig. 4).

### Anthropogenic land consolidation and interspecific competition shape the rodent community composition

To explore the possible causes of composition changes in the rodent community, we investigated the potential interactions between species and the impact of land consolidation (change in mean patch size) on the population dynamics of three numerically dominant local rodent species: striped field mouse, Norway rat (*Rattus norvegicus*) and buff-breasted rat (*Rattus flavipectus*). These three species represent 88% of all recorded rodents in the region. Our analysis using convergent cross-mapping (CCM)<sup>50</sup> revealed the presence of statistically significant interactions among the rodent populations (Fig. 2 and Supplementary Table 2). The results suggest that the striped field mouse affects Norway rat (Fig. 2a) and buff-breasted rat (Fig. 2b) populations, respectively. However, the Norway rat and the buff-breasted rat do not show an effect on the striped field mouse. The buff-breasted rat also has an effect on the Norway rat but not vice versa (Fig. 2c). Further interaction relationships between the other six species are shown in Supplementary Fig. 4.

Next, we fitted the distributed lag nonlinear model (DLNM)<sup>51</sup> to analyse the potential nonlinear association between rodent population dynamics and land consolidation, while also considering the confounders of climate variables, intraspecific and interspecific competition. To reduce complexity and uncertainty, these three rodent species were modelled separately. Our statistical analysis suggested that climate, intraspecific and interspecific competition and land consolidation played a crucial role in the rodent population dynamics. Moreover, the mean patch size was found to be positively associated with the population density of the striped field mouse, negatively associated with the Norway rat but not associated with that of the buff-breasted rat (Fig. 3).

### Anthropogenic land consolidation affects species competition and virus transmission

To further explore the interactive effect of land consolidation and species competition in the rodent community, we constructed a discrete nonlinear time-series model based on Lotka–Volterra dynamics<sup>52</sup>. Specifically, we analysed the effects of climate, land consolidation and species competition on the rodent community structure in this model (Methods). The model allowed us to estimate the effect of land consolidation ( $\tau$ ) on intraspecific and interspecific competition intensity using time-series data from the three rodent populations (Fig. 4b). Higher values of  $\tau$  correspond to a stronger intensity of the effect, while the sign of  $\tau$  indicates a positive or negative effect on species competition. Our results revealed that land consolidation has lasting and time-varying effects on species competition. The cumulative effect is positive for the striped field mouse but negative for both the Norway rat and buff-breasted rat (Fig. 4d). Furthermore, land consolidation intensifies the interspecific competition among rodent species (Fig. 4e,g and Supplementary Fig. 6). Thus, our analysis strongly suggests that land consolidation leads to changes in intraspecific and interspecific competition; and those changes, at least in part, further lead to the observed shifts in species composition of the rodent community. As such, our models predict that increasing speeds of land consolidation will lead to a decline in the rodent population growth rate (Supplementary Fig. 7). We also performed sensitivity analyses by

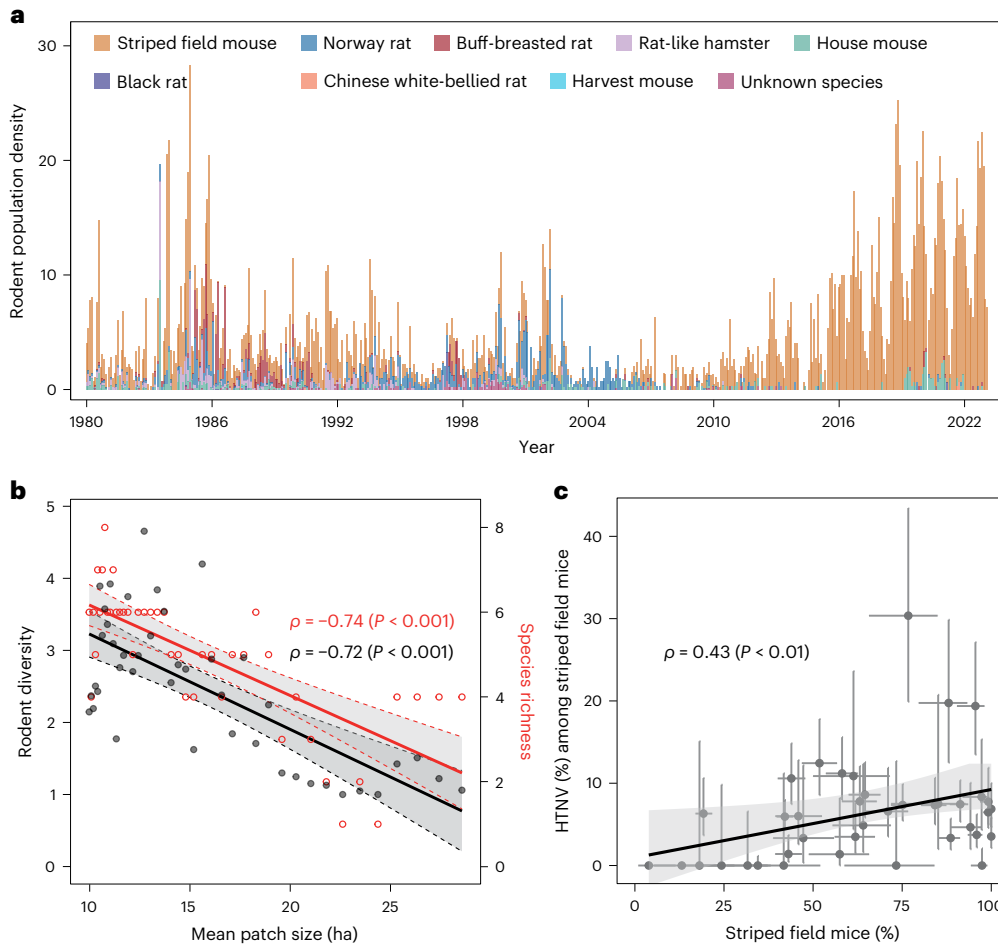


**Fig. 1 | Observed dynamics of rodent diversity, community composition and HTNV prevalence among striped field mice, 1980–2022, the Hu region, China.** **a**, Rodent community composition. Rodent population density for each species is expressed as capture numbers in 100 trap nights. **b**, Rodent species diversity decreased with mean land patch size. The scatterplot shows the association between mean patch size and rodent species diversity (left y axis, black dots, effective number of species) and between mean patch size and species richness (right y axis, red circles, species richness), assessed with Spearman’s rank correlation coefficient ( $\rho$ ). The correlations are significant

( $P < 0.001$ , two-sided test). Lines represent fitted linear regression models (shading shows 95% confidence intervals of fitted values). The mean patch size for each year was interpolated from the observed values using generalized additive models (Supplementary Fig. 2). **c**, HTNV prevalence among striped field mice increases with the percentage of striped field mice comprising the rodent community. The correlation between them was evaluated with Spearman’s rank correlation coefficient ( $\rho$ ) and found to be significant ( $P = 0.0061$ , two-sided test). Error bars represent 95% credible intervals.

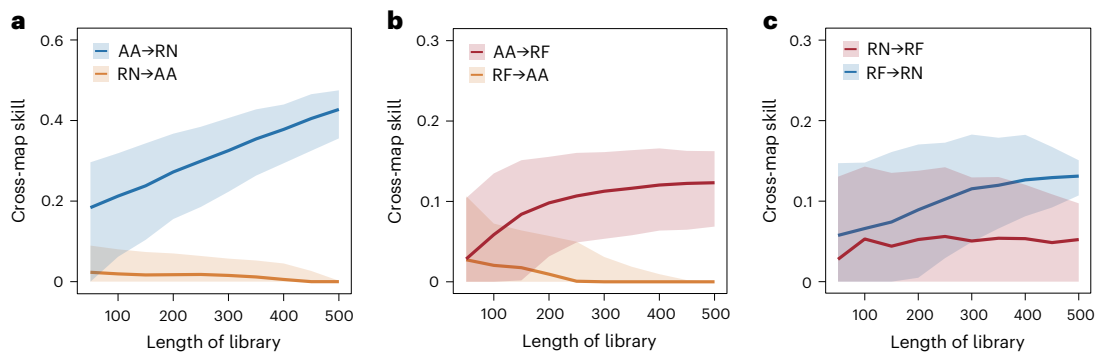


**Fig. 2 | Detecting interspecific causality in rodent population dynamics.** **a–c**, Interactions between striped field mice (AA) (**a**), Norway rat (RN) (**b**) and buff-breasted rat (RF) (**c**). The strength of the interaction between each pair of rodent species was assessed with the CCM skill, of which the value ranges from 0 to 1. Solid lines represent the mean of cross-mapping skill of each library size. Shaded regions represent the 95% credible intervals. AA → RN, the effect of

species AA on species RN and so on. Length of library refers to the number of data points used to construct the mapping. Cross-map skill is Pearson’s correlation coefficient ( $\rho$ ) between the predicted driver values, obtained using the univariate state-space reconstruction of the response variable and the observed driver values. The better the cross-map estimate, the stronger causal effect in the response variable.

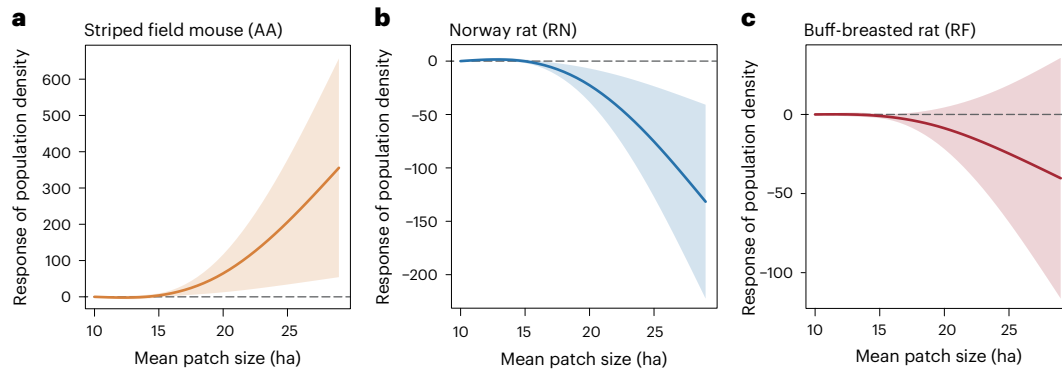


**Fig. 3 | Associations between land consolidation and rodent population dynamics.** a–c, Association between mean patch size and population dynamics of striped field mouse (AA) (a), Norway rat (RN) (b) and buff-breasted rat (RF) (c). Estimations of effects are based on DLNMs. Solid lines and shaded regions represent the estimation values and 95% credible intervals.

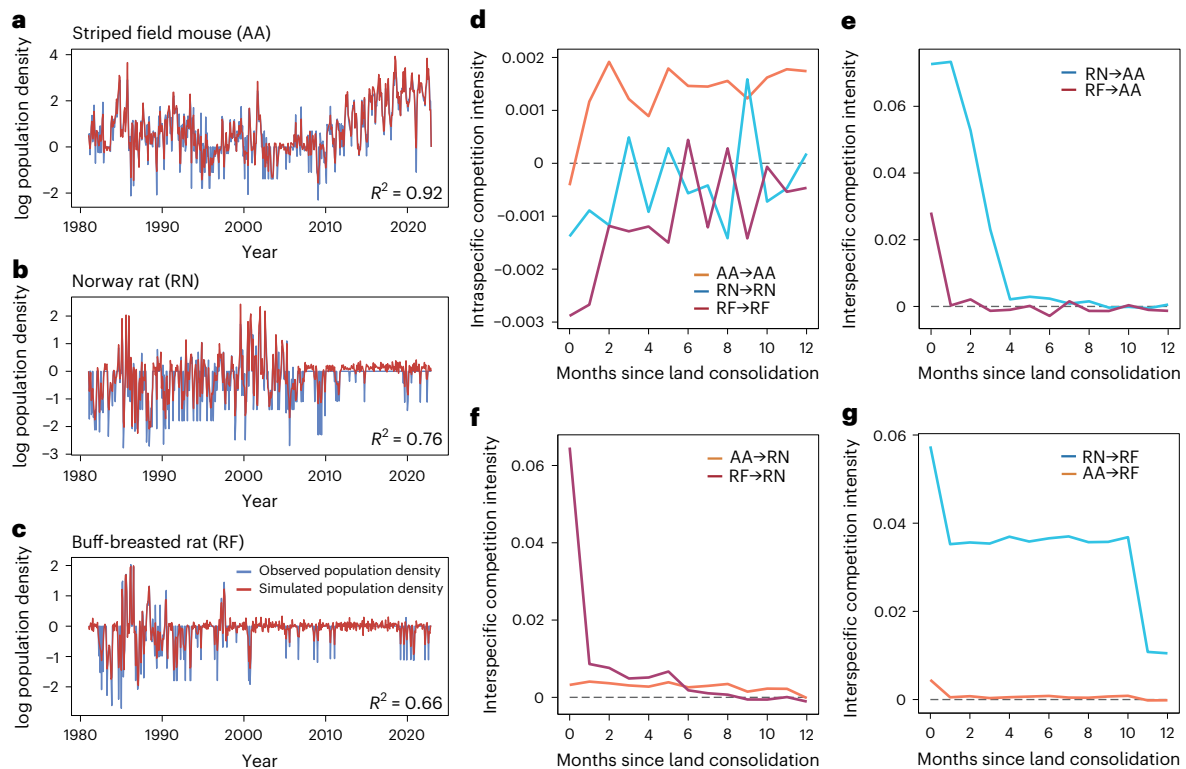


**Fig. 4 | Model simulations of the three-species dynamic model compared to empirical observations and parameter estimates from the three-species dynamic model.** a–c, Estimated rodent population density (red lines) and the observations (blue lines) for striped field mouse (AA) (a), Norway rat (RN) (b) and buff-breasted rat (RF) (c). Rodent population density for each species

is expressed as capture numbers per 100 trap nights. d, The effect of land consolidation on intraspecific competition. AA → AA is the effect of species AA on itself. e–g, The effect of land consolidation on interspecific competition intensity among species pairs: RN → AA and RF → AA (e), AA → RN and RF → RN (f), and RN → RF and AA → RF (g). RN → AA is the effect of species RN on species AA.

replacing the mean patch size with either the agriculture patch area or the urban patch area, modifying climatic variables and subsequently changing the speed of land consolidation. Additionally, as antirodent campaigns primarily target striped field mice that carry the HTNV in the Hu region, we conducted sensitivity analyses by increasing the population density of the striped field mouse by 20% and 50% (ref. 53). The effect of land consolidation on species competition remained the same (Supplementary Figs. 8–14).

As striped field mouse is the main reservoir of HTNV in the Hu region, with infected individuals accounting for >95% of all infected rodents, we next investigated whether anthropogenic land consolidation influences HTNV transmission among rodents based on a single-species epidemic model<sup>54,55</sup>. This model, which incorporates

temperature and rainfall as potential climatic factors and land consolidation as a driver of human activity, captures well the key features of the observed HTNV transmission dynamics (Fig. 5a and Methods). The results indicated that the impact of land consolidation on virus transmission changes from negative to positive over time (Fig. 5b). We inferred that increasing the patch size may reduce contacts between striped field mice in the initial months. As the striped field mouse exhibits strong survival abilities and becomes numerically dominant species with increased patch size, it amplifies the risk of HTNV transmission within the host reservoir.

Last, given the considerable irregular species replacement observed over the past decades, we estimated global and local Lyapunov exponents<sup>56,57</sup> to assess the potential presence of chaos in rodent

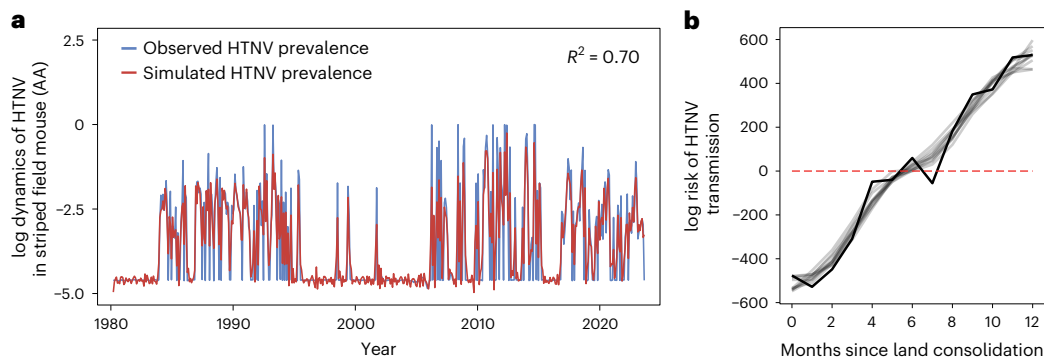


**Fig. 5 | Results of the nonlinear transmission model of HTNV among striped field mice.** **a**, Temporal dynamics of observed (blue line) and simulated HTNV prevalence (red line). HTNV prevalence represents the trend of HTNV carried proportion in the striped field mouse. **b**, The effect of land consolidation on

HTNV transmission (black line), that is  $\log \beta_{\text{patch}}$ . The ten curves in grey are a subset of the global confidence set for  $\log \beta_{\text{patch}}$  created by bootstrapping. Red line represents the baseline level of the effect of land consolidation on HTNV transmission.

community dynamics. A positive Lyapunov exponent represents the divergence of nearby trajectories, which is widely regarded as an indicator of chaos. The global Lyapunov exponent is related to the average rate of trajectory divergence or convergence over the entire dynamical system, whereas local Lyapunov exponents measure the rate of trajectory divergence or convergence over a short period of time. Our analysis yielded a positive global Lyapunov exponent of 4.39 and positive local Lyapunov exponents ranging from 2.0 to 14.6 for the entire rodent community (Supplementary Fig. 15), highlighting the intricacies inherent in this system. However, specifically for the striped field mouse, a negative global Lyapunov exponent of  $-0.65$  was observed and local Lyapunov exponents alternated between positive and negative values in the first 30 years, consistently converging to negative values within the subsequent 10 years. These findings suggested that the main host reservoir of HTNV experienced localized oscillations before eventually stabilizing to a robust steady state, influenced by the land consolidation process.

## Discussion

Our long-term, regional study reveals that anthropogenic land consolidation has been an ecologically disruptive process for local rodent communities in the Hu region of China, causing irregular species fluctuations by suppressing intraspecific and intensifying interspecific competition over the past four decades. Detecting chaos in time series of rodent population dynamics implies that there is no stable state in the overall dynamical system, which limits the predictability of zoonotic host abundances<sup>56</sup>. Despite the fact that synanthropic rodents act as virus reservoirs or transmitters in disease transmission<sup>58</sup>, little is known about their long-term population trends. Previous studies have shown that land-use and cultivation activities have little impact on the population growth rate or population dynamics of rodents<sup>59,60</sup>. Other studies have shown large differences in rodent population densities across large spatial scales but have been unable to link local densities to environmental drivers<sup>61</sup>. Furthermore, anthropogenic chemical interventions to reduce rodent population abundances<sup>62</sup>, while occasionally successful, often fail to achieve sustainable control.

Our findings also suggest that anthropogenic activities affect rodents not only directly (for example by affecting the rodent population growth rate) but also indirectly via interspecific competition. Interspecific competition is often difficult to measure and consequently has been largely neglected. Additionally, the indirect influence on rodents resulting from anthropogenic activities may only be detectable over long temporal scales, such as decades<sup>63</sup>. Here, we demonstrate that long-term monitoring of these rodent populations provides insights into the drivers of changes in the composition of synanthropic rodent

communities, which have key implications for mitigating the impacts of rodent populations on potential disease outbreak risks.

The dramatic decline in rodent biodiversity over the past four decades (that is, a notable shift in the rodent community composition) is associated with anthropogenic land-use change. In particular, the striped field mouse has benefited from land consolidation and has become the numerically dominant species at the community level. Our computational analysis indicates that the observed land-use change probably reflects the strong adaptability of the striped field mouse to changes in land use, which appears to exceed that of other rodent species. Striped field mice can flexibly adjust their behavioural response to both urban and rural environments<sup>64</sup> and exhibit demographic flexibility<sup>65</sup>. Consequently, they can tolerate human-modified landscapes and outcompete other rodent species, including invasive Norway rat. Similar patterns have been observed for other animal communities in human-managed ecosystems, such as bird and gecko communities<sup>66,67</sup>. However, as our inference is based on statistical analysis of time-series data, further experiments will be necessary to examine and validate these findings.

An alternative explanation is that the anthropogenic land-use change affects the three most abundant rodent species differently and consequently alters the structure of interspecific competition among them. For example, Norway rats live on agricultural and urban land-use types, while striped field mice prefer mainly agricultural land. As overall sanitation and infrastructure in the urban area of the Hu region has improved considerably, Norway rats were more severely impacted than striped field mice. Furthermore, our observations of the rodent community composition are particularly striking, since the rodent community over the study period consisted exclusively of synanthropic species, for which life histories are fast-paced and have a relatively higher tolerance towards human activities.

The striped field mouse, the main benefactor of the land consolidation process, is also the main host reservoir for HTNV. HTNV is an important zoonotic pathogen that causes HFRS, where China has the highest global incidence<sup>44,45</sup>. Previous studies have suggested an association between biodiversity and rodent-borne diseases, where a higher virus prevalence is generally observed in areas with lower rodent biodiversity<sup>68,69</sup>. Our observation that the prevalence of HTNV among striped field mice increased with lower rodent diversity is therefore consistent with these studies. Other studies have shown that changes in landscape structure can foster transmission risk by increasing HTNV reservoir species abundance<sup>70,71</sup>. Nevertheless, our findings indicate a growing zoonotic risk stemming from anthropogenic land-use change within the rodent community. To the best of our knowledge, such a mechanism has rarely been reported.

Our study highlights the critical need to understand a broader context of the ecological responses associated with land-use change.

Despite having access to unique long-term field data on rodent community composition, gaps remain in our understanding of rodent population ecology. Specifically, the marked decline and subsequent resurgence of rodent population abundance, coupled with the observed numerical dominance of the Norway rat over striped field mice in the early 2000s, remain unexplained by existing models, highlighting potential unaccounted drivers of synanthropic rodent population dynamics. Furthermore, limitations of the data prevent us from introducing replication tests to strengthen the results, such as the lack of data on rodents captured for each trapping site. Understanding the cause of these variations in rodent populations is essential to control and prevent future disease risk, which probably requires more intensive monitoring of local rodent communities.

We find that anthropogenic land consolidation, measured as an increase in patch size, influences species competition in synanthropic rodent communities. More broadly, our study sheds light on the complex interplay between human-mediated land-use change and rodent ecology. Moreover, other metrics of land consolidation, such as edge density and the distance between patches, may influence species dispersal and require further investigation. Other concurrent human activities along with the landscape–ecological consolidation process, such as agricultural mechanization, pest control and crop production, may also shape species-specific survival and reproduction. Thus, additional tests of these hypotheses on a fine scale will be necessary to forecast rodent responses to anthropogenic disturbance. Crucially, our study highlights the importance of systematic and long-term surveillance of various animal communities, especially in regions experiencing ongoing and substantial anthropogenic disturbances.

## Methods

### Study area and HFRS rodent host survey

Our study area, the Hu region (108.6° E, 34.1° N) in Shanxi province, Central China, is a predominantly agricultural county. The southern half of the county is an uninhabited mountain (Qinling), which is not included in this work. We focus on the northern part (Supplementary Fig. 2a), a plain with a total population of 597,100 in 2010, where 80% of the population is agricultural and 75% of the area is under agricultural use<sup>72</sup>. The Hu region was determined to be a national observation location for HFRS in around 1980 and since then monthly surveillance of local rodent abundance and human HFRS cases have been conducted regularly. Rodent trapping was carried out for three consecutive nights each month at each of the nine trapping sites located on agricultural land near residential areas. At each site, we deployed 100 traps (four parallel trap lines with 25 traps per line and 5 m spacing between traps). A total of 308,476 trap nights were conducted from 1980 to 2022, with a minimum of 300 trap nights per month. All trapped rodents were identified to species and the recorded species include striped field mouse, Norway rat, buff-breasted rat, rat-like hamster, house mouse, black rat, Chinese white-bellied rat, harvest mouse and unknown species.

To measure the diversity of rodent species, we calculated the Shannon–Wiener diversity index<sup>47</sup> and the effective number of species, a modified Shannon–Wiener diversity index, which is defined by the following formula<sup>46</sup>:

$$\text{effective number} = \exp\left(-\sum_{i=1}^n p_i \log(p_i)\right) \quad (1)$$

where  $n$  is the number of species and  $p_i$  is the proportion of species  $i$ .

### Land-use data

To monitor land-use changes in the Hu region, we acquired land-use classification product from 1980 to 2022, every 5 years, except 1985, from the Data Center for Resources and Environmental Sciences, Chinese Academy of Sciences (<http://www.resdc.cn>). Raw data were obtained from Landsat-MSS (1980) and Landsat-TM/ETM (1990–2022)

at a 30 m resolution. For the northern Hu region, we extracted the primary (level 1) land-use types (five in total), which includes forest, agricultural land, water, urban and unused areas. Since the rodents investigated in this study live mainly in agricultural and urban areas, land consolidation refers to agricultural and urban lands. It should be noted that the other three types of land use (water, forest and unused) have remained mostly unchanged over the last four decades and are not included in the study region (Box 1).

### Anthropogenic land consolidation

Land consolidation is an important step in urbanization, arising in association with social and economic development, including agricultural yield, human housing and taxation and infrastructure<sup>73</sup>. It is generally regarded as the reallocation and rearrangement of parcels, resulting in a larger patch size and less fragmentation for some land uses<sup>74</sup>. To trace the land consolidation process in the Hu region, we calculated the area of each patch for each land-use type using Fragstats 4.7 software. On the basis of standard area calculation algorithms, Fragstats 4.7 calculates the area of each patch by counting the number of pixels within the independent polygon shape of each patch and converting it into the desired area unit. For each land-use type, annual land-use data were interpolated using the generalized additive model, with a deviance explanation of models >90%. Regarding the average area available for rodent populations inhabiting urban and agricultural landscapes, we calculated the mean patch size of urban and agricultural land area, respectively, as the two types of habitat patch size ( $A$ ). For each year, the mean patch size is calculated as follows:

$$A = \frac{\sum_{i=1}^{n_{\text{urb}}} A_{\text{urb},i} + \sum_{i=1}^{n_{\text{agr}}} A_{\text{agr},i}}{n_{\text{urb}} + n_{\text{agr}}} \quad (2)$$

where  $n$  represents the patch number and  $A_i$  represents the area for patch  $i$ . The subscripts represent the land-use type (urb denotes urban and agr agricultural land).

Edge density is defined as the length of edges between heterogeneous landscape elements per unit area within a landscape. We calculated the edge length of each patch using ArcMap 10.7 software and aggregated these lengths to obtain the total edge length. A buffer radius of 0.5 km was established around each patch to determine the area of the buffer zones and the total patch area was calculated as the sum of all these buffer zones. Edge density was then computed as the ratio of total edge length to total patch area. The distance between patches was quantified as the average nearest-neighbour distance between patches. For each patch, we identified its nearest neighbouring patch, calculated the distances to these nearest neighbours and then computed the average of these distances to represent the distance between patches.

### Climate data

The monthly average temperature and rainfall data were obtained from the Hu County meteorological station from 1980 to 2020 and world weather online from 2021 to 2022 (<https://www.worldweatheronline.com/huxian-weather-averages/shaanxi/cn.aspx>).

### Multiple linear regression

To identify factors influencing response variable such as HTNV transmission, we used multiple linear regression to estimate the association between variables. The multiple regression model is given by:

$$Y_t = \alpha + \beta_1 \text{patchsize}_t + \beta_2 \text{AAdensity}_{t-1} + \beta_3 \text{temperature}_t + \beta_4 \text{rainfall}_t + \epsilon \quad (3)$$

where  $Y_t$  is the prevalence of HTNV on month  $t$ . Parameter  $\alpha$  is the intercept of the regression model and  $\beta_1$ ,  $\beta_2$ ,  $\beta_3$  and  $\beta_4$  represent the coefficients of variables. Parameters temperature <sub>$t$</sub> , rainfall <sub>$t$</sub> , and patchsize <sub>$t$</sub>  represent temperature, rainfall and mean patch size on month  $t$ ,

respectively.  $AA_{density}_{t-1}$  is the AA density on month  $t - 1$ . Parameter  $\epsilon$  is the random error. To further consider the effect of edge density and the distance between patches on HTNV transmission, we also incorporated these two variables into the regression model.

**Structural equation model**

To further examine the relationship between land consolidation, climate factors, species diversity and disease transmission within a single model framework, we used SEM<sup>49</sup> as an integrated approach to estimate the structural correlation between variables. SEM was performed using the R package lavaan<sup>75</sup> with maximum likelihood estimation procedures.

**Interactions between rodent species**

To preliminarily explore potential relationships in the rodent community, we applied the CCM method<sup>50</sup> to the time series of the population abundance of three numerically dominant rodent species (Fig. 2a). CCM is a statistical method based on space state reconstruction, representing the statistical link between the value of variable  $X$  reconstructed by the other variable  $Y$  (using the nearest-neighbour forecasting method) and the observed value  $X$  as cross-map skill. It can be used to detect weak interactions in nonlinear systems, such as ecosystems, where interactions among species are often weak to moderate<sup>50</sup>. In particular, the CCM can distinguish the interactions between species and the effect caused by other shared driving factors<sup>50</sup>, making it an ideal tool for our case. The critical criterion for estimating causal interactions between two variables using CCM is to ensure that the cross-mapping skill monotonically increases and converges with the length of time series used in cross-mapping. Here, CCM was adopted to assess the causal strength between time series of population abundance of three numerically dominant rodent species, measuring the degree to which changes in the abundance of each rodent species are attributable to changes in the abundance of the other species. For each pair of species, we computed cross-map skills to show the strength of interactions. We also provided a null expectation by running the causality test on the surrogate time series using the method of ‘seasonal’ (Supplementary Table 2). The analyses were performed using the rEDM package (v.1.14.3) of R (v.4.3.1)<sup>76,77</sup>. In the analysis, the embedding dimension ( $E$ ) was set according to the results of the simplex projection.

**The effect of anthropogenic land consolidation on rodent population density**

Among all rodents recorded in our study, striped field mice, Norway rats and buff-breasted rats together account for 88% of the total number of rodents. Consequently, instead of including all rodent species in our analysis, we focus on these three numerically dominant rodent species. To explore the potential nonlinear association between land consolidation and population dynamics of the three numerically dominant rodent species, we applied the DLNM<sup>51</sup>. The DLNM framework is based on the definition of the cross-basis function, which can combine the lag–response function and exposure–response function to describe the nonlinearity and lag correlation simultaneously. Specifically, the lag–response functions for each covariate are constructed using the natural cubic splines with 4 degrees of freedom and the maximum lag was specified up to 24 for all variables, except for mean patch size, and the maximum lag was set as 48 for mean patch size. Therefore, we can fit the nonlinear lag–response relationship between rodent population dynamics and land consolidation over the cumulative lag of 48 months. Time-series analysis was performed with the R packages dlnm, mgcv and splines. The regression model is given by:

$$Y_t = \alpha + \beta_1 cb.AAdensity_t + \beta_2 cb.RNdensity_t + \beta_3 cb.RFdensity_t + \beta_4 cb.temperature_t + \beta_5 cb.rainfall_t + \beta_6 cb.patchsize_t + month, \tag{4}$$

where the error term follows the Gaussian distribution.  $Y_t$  is the monthly population density for AA, RN and RF on month  $t$ . Parameter  $\alpha$  is the intercept of the regression model and  $\beta_1, \beta_2, \beta_3, \beta_4, \beta_5$  and  $\beta_6$  are the coefficients of covariates.  $cb.AAdensity_t, cb.RNdensity_t, cb.RFdensity_t, cb.temperature_t, cb.rainfall_t$  and  $cb.patchsize_t$  represent the cross-basis functions for the AA density, RN density, RF density, temperature, rainfall and mean patch size on month  $t$ , respectively. The remaining variables are seasonal control variables.

**Three-species population dynamic model**

Although CCM was used to preliminarily explore causal relationships among the three numerically dominant rodent species, it cannot directly identify the positive or negative nature of a relationship, nor can it determine the strength of the interactions. To further investigate the interactive effects of species competition within the rodent community and how these effects are influenced by mean patch size, we constructed a multispecies population dynamics model (based on Lotka–Volterra equations<sup>52</sup>), considering intrinsic growth rate of rodent population and species competition among them (Fig. 4). Competition among rodent species manifests as the occupation of resources. We focus on population densities of striped field mice, Norway rat and buff-breasted rats, which together comprise 88% of the total number of rodents in our study. The population abundance was represented by the number of rodents caught per 100 trap nights.

$$\dot{N}_{i,t+1} = N_{i,t} \left( r_{i,t} - \sum_{j=1} F_{j,t} N_{j,t} \right) \tag{5}$$

where  $N_{i,t}$  (with  $i = AA, RN, RF$ ) represents the abundance of species  $i$  at time  $t$ . Parameter  $r_{i,t}$  is the intrinsic growth rate of population  $i$ , respectively.  $F_{j,t}$  represents the intraspecific or interspecific competition effect of species  $j$  on species  $i$  at time  $t$ .

Previous researchers have reported several relationships between patch size and population abundance, including positive<sup>78</sup>, negative and none<sup>79,80</sup>. Different species have different habitat preferences between patches of different sizes. This preference would lead to more resource occupation, thus forming a competitive advantage among the community. However, to our knowledge, there is no evidence on the preference for patch size of rodents living in the Hu region. Therefore, we formulate a simple model for species competition, equation (5), assuming that the competition coefficient is linearly related to the patch size preference.  $A_t$  is the mean patch size of the habitat at time  $t$ .  $\tau_j$  and  $\epsilon_j$  are the scale factor and the intercept, respectively, to quantify the effect of the patch size change on the resource occupation of species  $j$ . Here, the sign of  $\tau$  shows the direction of the effect, that is to intensify or weaken the species competition effect; and the magnitude of  $\tau$  shows the strength of the effect.

$$F_{j,t} = \tau_j A_t + \epsilon_j \tag{6}$$

We consider that the intrinsic growth rate ( $r_{i,t}$ ) of population  $i$  over time contains both long-term trends and seasonal fluctuations component in our model, that is  $r_{i,t} = r_{i,lt} + r_{i,seas}$ , where  $r_{i,seas}$  contains environment influence components from temperature and rainfall, that is  $r_{i,rain} \Delta_i Rain$  and  $r_{i,temp} \Delta_i Temp$ . Parameters  $r_{i,rain}$  and  $r_{i,temp}$  are composed of  $n = 12$  distinct values, one for every month.  $\Delta$  is a vector of dummy variables with a length of  $n - 1$ . Specifically, the intrinsic growth rate of population  $i$  is given by:

$$r_{i,t} = r_{i,lt} + \sum_{j=1}^{n-1} (r_{i,rain})_j \Delta_{j,t} Rain_{t-2} + \sum_{j=1}^{n-1} (r_{i,temp})_j \Delta_{j,t} Temp_{t-2} \tag{7}$$

Substituting equations (6) and (7) into equation (5), the equation can be written as:

$$\frac{\hat{N}_{i,t}}{N_{i,t}} = (\log N_{i,t})' = r_{i,t} + \sum_{j=1}^{n-1} (r_{i,\text{rain}})_j \Delta_{j,t} \text{Rain}_{t-2} + \sum_{j=1}^{n-1} (r_{i,\text{temp}})_j \Delta_{j,t} \text{Temp}_{t-2} - \sum_{i=1}^3 \sum_{k=0}^m (\tau_{i,k} A_{t-k} + \varepsilon_{i,k}) N_{i,t-k} \tag{8}$$

Assume that  $\Delta t$  is 1 month, then  $(\log N_{i,t})' = \frac{d(\log N_{i,t})}{dt} = \log N_{i,t} - \log N_{i,t-1}$ . Furthermore, equation (7) can be written as a semiparametric additive model<sup>45,46</sup>:

$$\log N_{i,t} - \log N_{i,t-1} = r_{i,t} + \sum_{j=1}^{n-1} (r_{i,\text{rain}})_j \Delta_{j,t} \text{Rain}_{t-2} + \sum_{j=1}^{n-1} (r_{i,\text{temp}})_j \Delta_{j,t} \text{Temp}_{t-2} - \sum_{i=1}^3 \sum_{k=0}^m (\tau_{i,k} A_{t-k} + \varepsilon_{i,k}) N_{i,t-k} \tag{9}$$

Using a backfitting algorithm, the parametric part of the model is first fitted through weighted least-squares regressions. The backfitting algorithm is applied to provide a progressive improvement in our estimate of the interspecific competitive in the population through the adjustment of parameter  $\tau$ . The nonparametric part of the model—this is the long-term intrinsic growth rate of the rodent population—is then obtained by smoothing the residuals of the regression step. The smoothing bandwidth  $h = 1$  and the spline penalty weight  $\mu = -5$  in AA, RN and RF fitting model. The specific fitting process is as follows:

Letting the row vector  $X_t = [\Delta_t \text{Rain}_{t-2}, \Delta_t \text{Temp}_{t-2}, N_{\text{AA},t}, N_{\text{RN},t}, N_{\text{RF},t}, t, U, V, W]$  where  $\Delta_t = (\Delta_{1,t}, \Delta_{2,t}, \dots, \Delta_{n-1,t})$  and  $(U, V, W) = -(\text{Patch}_t N_{\text{AA},t}, \text{Patch}_t N_{\text{RN},t}, \text{Patch}_t N_{\text{RF},t})$  the parametric part of equation (8) can be solved as:

$$\hat{\theta} = (X^T (I - W) X)^{-1} X^T (I - W) Y \tag{10}$$

where  $X$  is a matrix with rows  $X_t$ ,  $Y$  is a column vector with row values  $\log(Y_{t+1}) - \log(Y_t)$ ,  $I$  is the identity matrix of size  $t \times t$ . As in the original method<sup>55</sup>, we use a truncated Gaussian kernel with a specified smoothing bandwidth  $h$  in the construction of the weight matrix  $W$ . The resulting regression coefficients are  $\hat{\theta} = [r_{\text{rain}}, r_{\text{temp}}, \varepsilon, \tau]^T$ , where  $r_{\text{rain}} = (r_{\text{rain},1}, r_{\text{rain},2}, \dots, r_{\text{rain},n-1})$ ,  $r_{\text{temp}} = (r_{\text{temp},1}, r_{\text{temp},2}, \dots, r_{\text{temp},n-1})$ ,  $\varepsilon = (\varepsilon_{1,0}, \varepsilon_{1,1}, \dots, \varepsilon_{1,m}, \varepsilon_{2,0}, \varepsilon_{2,1}, \dots, \varepsilon_{2,m}, \varepsilon_{3,0}, \varepsilon_{3,1}, \dots, \varepsilon_{3,m})$  and  $\tau = (\tau_{1,0}, \tau_{1,1}, \dots, \tau_{1,m}, \tau_{2,0}, \tau_{2,1}, \dots, \tau_{2,m}, \tau_{3,0}, \tau_{3,1}, \dots, \tau_{3,m})$ . The  $\tau$  values are then fitted with a penalized cubic regression spline (with ten knots and a penalty weight  $\mu$ ) that is constrained to be monotonically decreasing and positive.

The initial estimated term is then calculated as:

$$\hat{Y}_t = Y_t - (U, V, W)^T \hat{\tau} \tag{11}$$

where  $\hat{\tau}$  is the spline-fitted coefficient. Now, we use a backfitting algorithm to obtain better parameter estimates for  $\hat{\tau}$ . Equation (9) becomes:

$$\hat{Y}_t = r_{i,t} + \sum_{j=1}^{n-1} (r_{i,\text{rain}})_j \Delta_{j,t} \text{Rain}_{t-2} + \sum_{j=1}^{n-1} (r_{i,\text{temp}})_j \Delta_{j,t} \text{Temp}_{t-2} - \sum_{i=1}^3 \sum_{k=0}^m \varepsilon_{i,k} N_{i,t-k} \tag{12}$$

Equation (12) is then through a weighted least-squares regression, similar to equation (9). Redefining the row vectors  $X_t = [\Delta_t \text{Rain}_{t-2}, \Delta_t \text{Temp}_{t-2}, A, \log I_t, \log(1 - I_t)]$ , where  $\Delta_t = (\Delta_{1,t}, \Delta_{2,t}, \dots, \Delta_{n-1,t})$ ,  $A = (A_t, A_{t-1}, \dots, A_{t-m})$  and  $I_t$  is virus carried rate at time  $t$ . The parametric part of equation (18) can be solved as:

$$\psi = (Z^T (I - W) Z)^{-1} Z^T (I - W) \rho \tag{13}$$

where  $\psi = (\psi_0, \psi_1, \dots, \psi_m)^T$ . The improved estimate  $\tau'$  can be written as:

$$\tau'_i = \hat{\tau}_i + \psi_i \text{ for } i = 0, 1, \dots, m. \tag{14}$$

These  $\tau'$  values are fitted with a constrained penalized regression spline as above, yielding the new estimate,  $\hat{\tau}'$ . The next iteration begins with replacing  $\hat{\tau}$  with  $\hat{\tau}'$ . By repeating backfitting algorithm, the  $\hat{\tau}$  value can be improved.

The second step of the semiparameter method is to obtain the  $r_{i,t}$  values from the resulting residuals by smoothing them with the  $W$  matrix:

$$r_{i,t} = W(Y - X\hat{\theta}) \tag{15}$$

where  $X$  is a matrix with rows  $X_t = [\Delta_t \text{Rain}_{t-2}, \Delta_t \text{Temp}_{t-2}, N_{\text{AA},t}, N_{\text{RN},t}, N_{\text{RF},t}]$ ,  $Y_t = \log(Y_{t+1}) - \log(Y_t) - (U, V, W)^T \hat{\tau}$ ,  $\hat{\theta} = [r_{\text{rain}}, r_{\text{temp}}, \varepsilon]^T$ .

### Transmission equation for HTNV prevalence

To investigate the effect of anthropogenic land consolidation on the dynamics of zoonotic HTNV, a discrete nonlinear transmission equation was constructed on the basis of a single-species epidemic model, as the striped field mouse is the main reservoir host for HTNV, with infected individuals accounting for >95% of all infected rodents in the study area. This model incorporates temperature, rainfall and land consolidation as drivers. The form of transmission equation is as follows:

$$I_{t+1} = \beta_t I_t^{\alpha} S_t^{\gamma} \varepsilon_t, \tag{16}$$

where  $I$  is the proportion of the striped field mouse that carries HTNV.  $S$  is the proportion of susceptible population.  $\beta_t$  is pathogen transmissibility over time.  $\varepsilon_t$  is the multiplicative noise. We consider that pathogen transmissibility  $\beta_t$  is the product of three separate components: a long-term one,  $\beta_{\text{lt}}$ , a seasonal one,  $\beta_{\text{seas}}$ , and a patch-affected one,  $\beta_{\text{patch}}$ . Equation (16) becomes:

$$I_{t+1} = \beta_{\text{lt}} \beta_{\text{seas}} \beta_{\text{patch}} I_t^{\alpha} (1 - I_t)^{\gamma} \varepsilon_t \tag{17}$$

where  $\beta_{\text{seas}}$  contains environment influence components from temperature and rainfall, that is  $\beta_{\text{rain}} \Delta \text{Rain}$  and  $\beta_{\text{temp}} \Delta \text{Temp}$ .  $\beta_{\text{rain}}$  and  $\beta_{\text{temp}}$  are composed of  $n = 12$  distinct values, one for every month.  $\Delta$  is a vector of dummy variables with a length of  $n - 1$ . The exponents  $\alpha$  and  $\gamma$  are mixing parameters included to allow for nonlinearities in contact rates. To fit the model, we log-transform equation (17), which becomes:

$$\log I_{t+1} = \log(\beta_{\text{lt}}) + \sum_{j=1}^{n-1} \log(\beta_{\text{Rain}})_j \Delta_{j,t} \text{Rain}_{t-2} + \sum_{j=1}^{n-1} \log(\beta_{\text{Temp}})_j \Delta_{j,t} \text{Temp}_{t-2} + \sum_{j=0}^m \log(\beta_{\text{patch}})_j A_{t-j} + \alpha \log(I_t) + \gamma [\log(1 - I_t)] + \log(\varepsilon_t) \tag{18}$$

The fitting method is similar to equation (9)<sup>55</sup>. Using the backfitting algorithm, the parametric part of the equation (18) is first fitted through weighted least-squares regressions. Letting the row vector  $X_t = [\Delta_t \text{Rain}_{t-2}, \Delta_t \text{Temp}_{t-2}, A, \log I_t, \log(1 - I_t)]$ , where  $\Delta_t = (\Delta_{1,t}, \Delta_{2,t}, \dots, \Delta_{n-1,t})$ ,  $A = (A_t, A_{t-1}, \dots, A_{t-m})$  and  $I_t$  is virus carried rate at time  $t$ . The parametric part of equation (18) can be solved as:

$$\hat{\theta} = (X^T (U - W) X)^{-1} X^T (U - W) Y \tag{19}$$

where  $X$  is a matrix with rows  $X_t$ ,  $Y$  is a column vector with row values  $\log I_{t+1}$ , and  $U$  is the identity matrix of size  $t \times t$ . As in the original

method<sup>55</sup>, we use a truncated Gaussian kernel with a specified smoothing bandwidth  $h$  in the construction of the weight matrix  $W$ . The resulting regression coefficients are  $\hat{\theta} = [\log \beta_{\text{rain}}, \log \beta_{\text{temp}}, \log \beta_{\text{patch}}, \alpha, \gamma]^T$ , where  $\log \beta_{\text{rain}} = (\log \beta_{\text{rain},1}, \log \beta_{\text{rain},2}, \dots, \log \beta_{\text{rain},n-1})$ ,  $\log \beta_{\text{temp}} = (\log \beta_{\text{temp},1}, \log \beta_{\text{temp},2}, \dots, \log \beta_{\text{temp},n-1})$  and  $\log \beta_{\text{patch}} = (\log \beta_{\text{patch},0}, \log \beta_{\text{patch},1}, \dots, \log \beta_{\text{patch},m})$ . The  $\log \beta_{\text{patch}}$  values are then fitted with a cubic regression spline. The initial estimated term is calculated as:

$$\hat{Y}_t = Y_t - \log \hat{\beta}_{\text{patch}} A \quad (20)$$

where  $\log \hat{\beta}_{\text{patch}}$  is the spline-fitted coefficient. Now, using the backfitting algorithm to get better parameter estimates for  $\log \hat{\beta}_{\text{patch}}$ . Equation (18) becomes:

$$\hat{Y}_t = \log(\beta_{it}) + \sum_{j=1}^{n-1} \log(\beta_{\text{rain},j}) \Delta_{j,t} \text{Rain}_{t-2} + \sum_{j=1}^{n-1} \log(\beta_{\text{temp},j}) \Delta_{j,t} \text{Temp}_{t-2} + \alpha \log(I_t) + \gamma [\log(1 - I_t)] \quad (21)$$

Equation (21) is then calculated through a weighted least-squares regression, similar to equation (18). Redefining the row vectors  $X_t = [\Delta_t \text{Rain}_{t-2}, \Delta_t \text{Temp}_{t-2}, \log I_t, \log(1 - I_t)]$  and  $Y_t = \hat{Y}_t$ , we get  $\hat{\theta} = (X^T (U - W) X)^{-1} X^T (U - W) Y = [\log \beta_{\text{rain}}, \log \beta_{\text{temp}}, \alpha, \gamma]^T$ . The residuals of this fit are  $\rho = Y - X\hat{\theta}$ . We can progressively improve the estimates of  $\log \hat{\beta}_{\text{patch}}$ . For the estimate of  $\log \hat{\beta}_{\text{patch}}$ , we have

$$\psi = (A^T (U - W) A)^{-1} A^T (U - W) \rho \quad (22)$$

where  $\psi = (\psi_0, \psi_1, \dots, \psi_m)^T$ . The improved estimate  $\log \beta'_{\text{patch}}$  can be written as:

$$\log \beta'_{\text{patch},i} = \log \hat{\beta}_{\text{patch},i} + \psi_i \text{ for } i = 0, 1, \dots, m \quad (23)$$

These  $\log \beta'_{\text{patch}}$  values are fitted with a cubic regression spline as above, yielding the new estimate,  $\log \hat{\beta}'_{\text{patch}}$ . The next iteration begins with replacing  $\log \hat{\beta}_{\text{patch}}$  with  $\log \hat{\beta}'_{\text{patch}}$ . By repeating backfitting algorithm, the  $\log \hat{\beta}_{\text{patch}}$  value can be improved.

The second step of the semiparameter method is to obtain the  $\beta_{it}$  values from the resulting residuals by smoothing them with the  $W$  matrix:

$$\beta_{it} = W(Y - X\hat{\theta}) \quad (24)$$

where  $X$  is a matrix with rows  $X_t = [\Delta_t \text{Rain}_{t-2}, \Delta_t \text{Temp}_{t-2}, \log I_t, \log(1 - I_t)]$   $Y_t = \log I_{t+1} - \log \hat{\beta}_{\text{patch}} A$ ,  $\hat{\theta} = [\log \beta_{\text{rain}}, \log \beta_{\text{temp}}, \alpha, \gamma]^T$ .

### Global and local Lyapunov exponents

Lyapunov exponents (LE) are used to measure trajectory divergence (or convergence) of the deterministic skeleton of the model<sup>56,57</sup>. It is calculated as the limit of the logarithm of the product of the Jacobian matrix of the model fitted along the observed time-series trajectory:

$$\text{LE} = \frac{1}{N\Delta t} \log \|J_N J_{N-1} \dots J_1 u_0\| \quad (25)$$

where  $N$  is the number of data points in the time series,  $\| \cdot \|$  is the Euclidean vector norm and  $u_0$  is a unit vector. The Jacobian matrices include partial derivatives with respect to the intrinsic variables  $N_{AA}$ ,  $N_{RN}$  and  $N_{RF}$ .

The local Lyapunov exponent was also calculated from equation (25). Whereas the global Lyapunov exponent measures the average trajectory divergence over the entire attractor of the dynamical system, local Lyapunov exponent measures local trajectory divergence over short stretch of the time series. In our case, the local Lyapunov exponent calculated the local trajectory divergence over 6 months,

which corresponded to six consecutive data points ( $N = 6$ ) at time intervals of  $\Delta t = 1$  month.

### Reporting summary

Further information on research design is available in the Nature Portfolio Reporting Summary linked to this article.

### Data availability

All data are available in the main text or the Supplementary Information. Raw data are not publicly available and are protected due to confidentiality agreements, which were used under license for the current study but are available upon reasonable request to the corresponding author and with permission from the data provider (H.T.). The request will be responded to within 2 weeks.

### Code availability

Code files are available via GitHub at <https://github.com/huaiyutian/Hantaan-virus>.

### References

1. Wiens, J. A., Stenseth, N. C., Vanhorne, B. & Ims, R. A. Ecological mechanisms and landscape ecology. *Oikos* **66**, 369–380 (1993).
2. *Global Indicator Framework for the Sustainable Development Goals and targets of the 2030 Agenda for Sustainable Development* (United Nations, 2020).
3. Seto, K. C. & Pandey, B. Urban land use: central to building a sustainable future. *One Earth* **1**, 168–170 (2019).
4. Foley, J. A. et al. Global consequences of land use. *Science* **309**, 570–574 (2005).
5. Shochat, E., Warren, P. S., Faeth, S. H., McIntyre, N. E. & Hope, D. From patterns to emerging processes in mechanistic urban ecology. *Trends Ecol. Evol.* **21**, 186–191 (2006).
6. Faust, C. L. et al. Pathogen spillover during land conversion. *Ecol. Lett.* **21**, 471–483 (2018).
7. Gibb, R. et al. Zoonotic host diversity increases in human-dominated ecosystems. *Nature* **584**, 398–402 (2020).
8. Keesing, F. & Ostfeld, R. S. Impacts of biodiversity and biodiversity loss on zoonotic diseases. *Proc. Natl Acad. Sci. USA* **118**, e2023540118 (2021).
9. Keesing, F. et al. Impacts of biodiversity on the emergence and transmission of infectious diseases. *Nature* **468**, 647–652 (2010).
10. Reynolds, J. D. in *Macroecology Life Histories and Extinction Risk* (ed. Blackburn, T. M.) 195–217 (Blackwell Publishing, 2003).
11. Ostfeld, R. S. & Keesing, F. Species that can make us ill thrive in human habitats. *Nature* **584**, 346–347 (2020).
12. Essl, F. et al. Distribution patterns, range size and niche breadth of Austrian endemic plants. *Biol. Conserv.* **142**, 2547–2558 (2009).
13. Kotiaho, J. S., Kaitala, V., Komonen, A. & Päävinen, J. Predicting the risk of extinction from shared ecological characteristics. *Proc. Natl Acad. Sci. USA* **102**, 1963–1967 (2005).
14. Saupe, E. E. et al. Niche breadth and geographic range size as determinants of species survival on geological time scales. *Glob. Ecol. Biogeogr.* **24**, 1159–1169 (2015).
15. Shultz, S., Bradbury, R. B., Evans, K. L., Gregory, R. D. & Blackburn, T. M. Brain size and resource specialization predict long-term population trends in British birds. *Proc. R. Soc. B.* **272**, 2305–2311 (2005).
16. Walker, J. S. Resource use and rarity among frugivorous birds in a tropical rain forest on Sulawesi. *Biol. Conserv.* **130**, 60–69 (2006).
17. White, R. L. & Bennett, P. M. Elevational distribution and extinction risk in birds. *PLoS ONE* **10**, e0121849 (2015).
18. Liang, C. et al. Taxonomic, phylogenetic and functional homogenization of bird communities due to land use change. *Biol. Conserv.* **236**, 37–43 (2019).

19. Colléony, A. & Shwartz, A. When the winners are the losers: invasive alien bird species outcompete the native winners in the biotic homogenization process. *Biol. Conserv.* **241**, 108314 (2020).
20. Safi, K. & Kerth, G. A comparative analysis of specialization and extinction risk in temperate-zone bats. *Conserv. Biol.* **18**, 1293–1303 (2004).
21. Boyles, J. G. & Storm, J. J. The perils of picky eating: dietary breadth is related to extinction risk in insectivorous bats. *PLoS ONE* **2**, e672 (2007).
22. McKinney, M. L. & Lockwood, J. L. Biotic homogenization: a few winners replacing many losers in the next mass extinction. *Trends Ecol. Evol.* **14**, 450–453 (1999).
23. Olden, J. D. Biotic homogenization: a new research agenda for conservation biogeography. *J. Biogeogr.* **33**, 2027–2039 (2006).
24. Olden, J. D. & Rooney, T. P. On defining and quantifying biotic homogenization. *Glob. Ecol. Biogeogr.* **15**, 113–120 (2006).
25. Clavel, J., Julliard, R. & Devictor, V. Worldwide decline of specialist species: toward a global functional homogenization? *Front. Ecol. Environ.* **9**, 222–228 (2011).
26. Li, D. et al. Changes in taxonomic and phylogenetic diversity in the Anthropocene. *Proc. R. Soc. B.* **287**, 20200777 (2020).
27. Jones, K. E. et al. Global trends in emerging infectious diseases. *Nature* **451**, 990–993 (2008).
28. Keesing, F., Holt, R. D. & Ostfeld, R. S. Effects of species diversity on disease risk. *Ecol. Lett.* **9**, 485–498 (2006).
29. Hansen, M. C. et al. High-resolution global maps of 21st-century forest cover change. *Science* **342**, 850–853 (2013).
30. Ceballos, G. et al. Accelerated modern human-induced species losses: entering the sixth mass extinction. *Sci. Adv.* **1**, e1400253 (2015).
31. Haddad, N. M. et al. Habitat fragmentation and its lasting impact on Earth's ecosystems. *Sci. Adv.* **1**, e1500052 (2015).
32. Ewers, R. M. et al. Logging cuts the functional importance of invertebrates in tropical rainforest. *Nat. Commun.* **6**, 6836 (2015).
33. Newbold, T. et al. Global effects of land use on local terrestrial biodiversity. *Nature* **520**, 45–50 (2015).
34. *The Sustainable Development Goals Report 2022* (UN DESA, 2022).
35. Fahrig, L. Effects of habitat fragmentation on biodiversity. *Annu. Rev. Ecol. Evol. Syst.* **34**, 487–515 (2003).
36. Ewers, R. M. & Didham, R. K. Confounding factors in the detection of species responses to habitat fragmentation. *Biol. Rev. Camb. Philos. Soc.* **81**, 117–142 (2006).
37. Zhou, Y., Li, Y. & Xu, C. Land consolidation and rural revitalization in China: mechanisms and paths. *Land Use Policy* **91**, 104379 (2020).
38. Tian, H. Y. et al. Urbanization prolongs hantavirus epidemics in cities. *Proc. Natl Acad. Sci. USA* **115**, 4707–4712 (2018).
39. Lin, Y., Han, G., Zhao, M. & Chang, S. X. Spatial vegetation patterns as early signs of desertification: a case study of a desert steppe in Inner Mongolia, China. *Landsc. Ecol.* **25**, 1519–1527 (2010).
40. Uchida, K. & Ushimaru, A. Biodiversity declines due to abandonment and intensification of agricultural lands: patterns and mechanisms. *Ecol. Monogr.* **84**, 637–658 (2014).
41. Maskell, L. C. et al. Exploring relationships between land use intensity, habitat heterogeneity and biodiversity to identify and monitor areas of high nature value farming. *Biol. Conserv.* **231**, 30–38 (2019).
42. Denac, K. & Krmecl, P. Land consolidation negatively affects farmland bird diversity and conservation value. *J. Nat. Conserv.* **59**, 125934 (2021).
43. McGarigal, K. & Cushman, S. A. Comparative evaluation of experimental approaches to the study of habitat fragmentation effects. *Ecol. Appl.* **12**, 335–345 (2002).
44. Tian, H. et al. Interannual cycles of Hantaan virus outbreaks at the human–animal interface in Central China are controlled by temperature and rainfall. *Proc. Natl Acad. Sci. USA* **114**, 8041–8046 (2017).
45. Fang, L. Z. et al. Reservoir host expansion of hantavirus, China. *Emerg. Infect. Dis.* **21**, 170–171 (2015).
46. Jost, L. Entropy and diversity. *Oikos* **113**, 363–375 (2006).
47. Pielou, E. C. Shannon's formula as a measure of specific diversity: its use and misuse. *Am. Nat.* **100**, 463–465 (1966).
48. Liu, Y., Yang, R. & Li, Y. Potential of land consolidation of hollowed villages under different urbanization scenarios in China. *J. Geogr. Sci.* **23**, 503–512 (2013).
49. Thakkar, J. J. in *Structural Equation Modelling* (ed. Kacprzyk, J.) 91–99 (Springer, 2020).
50. Sugihara, G. et al. Detecting causality in complex ecosystems. *Science* **338**, 496–500 (2012).
51. Gasparini, A. Modeling exposure–lag–response associations with distributed lag non-linear models. *Stat. Med.* **33**, 881–899 (2014).
52. Hofbauer, J. & Sigmund, K. *Evolutionary Games and Population Dynamics* (Cambridge Univ. Press, 1998).
53. Shilova, S. A. & Tchabovsky, A. V. Population response of rodents to control with rodenticides. *Curr. Zool.* **55**, 81–91 (2009).
54. Koelle, K. & Pascual, M. Disentangling extrinsic from intrinsic factors in disease dynamics: a nonlinear time series approach with an application to cholera. *Am. Nat.* **163**, 901–913 (2004).
55. Koelle, K., Rodó, X., Pascual, M., Yunus, M. & Mostafa, G. Refractory periods and climate forcing in cholera dynamics. *Nature* **436**, 696–700 (2005).
56. Benincà, E. et al. Chaos in a long-term experiment with a plankton community. *Nature* **451**, 822–825 (2008).
57. Benincà, E., Ballantine, B., Ellner, S. P. & Huisman, J. Species fluctuations sustained by a cyclic succession at the edge of chaos. *Proc. Natl Acad. Sci. USA* **112**, 6389–6394 (2015).
58. Gravinatti, M. L., Barbosa, C. M., Soares, R. M. & Gregori, F. Synanthropic rodents as virus reservoirs and transmitters. *Rev. Soc. Bras. Med. Trop.* **53**, e20190486 (2020).
59. Sluydts, V., Davis, S., Mercelis, S. & Leirs, H. Comparison of multimammate mouse (*Mastomys natalensis*) demography in monoculture and mosaic agricultural habitat: implications for pest management. *Crop Prot.* **28**, 647–654 (2009).
60. Mulungu, L. & Lopa, H. Comparative study of population dynamics and breeding patterns of *Mastomys natalensis* in system rice intensification and conventional rice production in irrigated rice ecosystems in Tanzania. *J. Rice Res.* **4**, 161 (2016).
61. Li, J., Liu, Q., Yang, T. & Wang, C. A three year monitoring program of countryside commensal rodent infestation in some towns and rural areas of China. *Chin. J. Vec. Biol. Contr.* **4**, 276–281 (1988).
62. Zhang, M., Wang, Y., Li, B., Guo, C. & Chen, A. Effects of chemical rodent control on rodent community structure in the Yangtze River Basin. *Acta Ecol. Sin.* **2**, 320–329 (2003).
63. Loreau, M. et al. Do not downplay biodiversity loss. *Nature* **601**, E27–E28 (2022).
64. Dammhahn, M., Mazza, V., Schirmer, A., Göttsche, C. & Eccard, J. A. Of city and village mice: behavioural adjustments of striped field mice to urban environments. *Sci. Rep.* **10**, 13056 (2020).
65. Tulis, F. et al. Expansion of the Striped field mouse (*Apodemus agrarius*) in the south-western Slovakia during 2010–2015. *Folia Oecol.* **43**, 753 (2016).
66. Shochat, E., Lerman, S. B., Katti, M. & Lewis, D. B. Linking optimal foraging behavior to bird community structure in an urban-desert landscape: field experiments with artificial food patches. *Am. Nat.* **164**, 232–243 (2004).
67. Petren, K. & Case, T. J. An experimental demonstration of exploitation competition in an ongoing invasion. *Ecology* **77**, 118–132 (1996).

68. Dizney, L. J. & Ruedas, L. A. Increased host species diversity and decreased prevalence of Sin Nombre virus. *Emerg. Infect. Dis.* **15**, 1012 (2009).
69. Dearing, M. D., Clay, C., Lehmer, E. & Dizney, L. The roles of community diversity and contact rates on pathogen prevalence. *J. Mammal.* **96**, 29–36 (2015).
70. Prist, P. R. et al. Landscape, environmental and social predictors of Hantavirus risk in São Paulo, Brazil. *PLoS ONE* **11**, e0163459 (2016).
71. Prist, P. R., D'Andrea, P. S. & Metzger, J. P. Landscape, climate and hantavirus cardiopulmonary syndrome outbreaks. *Ecohealth* **14**, 614–629 (2017).
72. *Shaanxi Statistical Yearbook 2010* (China Statistics Press, 2010).
73. Crecente, R., Alvarez, C. & Fra, U. Economic, social and environmental impact of land consolidation in Galicia. *Land Use Policy* **19**, 135–147 (2002).
74. Pašakarnis, G. & Maliene, V. Towards sustainable rural development in Central and Eastern Europe: applying land consolidation. *Land Use Policy* **27**, 545–549 (2010).
75. Rosseel, Y. lavaan: an R package for structural equation modeling. *J. Stat. Softw.* **48**, 1–36 (2012).
76. Park, J., Smith, C., Sugihara, G. & Deyle, E. rEDM: Empirical dynamic modeling ('EDM'). R package version 1.9.1 <https://CRAN.R-project.org/package=rEDM> (2021).
77. R Core Team *A Language and Environment for Statistical Computing* (R Foundation for Statistical Computing, 2021).
78. Kareiva, P. Finding and losing host plants by *Phyllotreta*: patch size and surrounding habitat. *Ecology* **66**, 1809–1816 (1985).
79. Bach, C. E. Effects of host plant patch size on herbivore density: underlying mechanisms. *Ecology* **69**, 1103–1117 (1988).
80. Bender, D. J., Contreras, T. A. & Fahrig, L. Habitat loss and population decline: a meta-analysis of the patch size effect. *Ecology* **79**, 517–533 (1998).
- Environmental Change Program (no. 2023-GC-ZYTS-11); and key research projects of Beijing Natural Science Foundation-Haidian District Joint Fund (L232014). J.R., O.G.P. and C.F. were funded by NSF/BBSRC project 'Integrating metaviromics with epidemiological dynamics: understanding virus transmission in the Anthropocene' (BB/Y006879/1). The funders had no role in study design, data collection and analysis, the decision to publish, or in preparation of the paper.

### Author contributions

H.T. conceived the study. H.T., O.G.P., A.P.D. and N.C.S. jointly supervised this work. P.Y., T.Z., J.Q. and J.W. collected the statistical data. S.P., Y.W., Y. Liang and Y.C. conducted the analyses. P.Y., J.R., Z.L., Q.L., C.S., G.D., C.L.F., J.Q., J.W., S.L., T.Z., C.M., N.B., B.C., R.Y., O.G.P., A.P.D., Y.X., Y. Li and N.C.S. edited the paper. H.T., S.P., Y.C., Y. Li, Y.W., Y.T. and J.R. wrote the paper. All authors read and approved the paper.

### Competing interests

The authors declare no competing interests.

### Additional information

**Supplementary information** The online version contains supplementary material available at <https://doi.org/10.1038/s41559-024-02570-x>.

**Correspondence and requests for materials** should be addressed to Pengbo Yu, Nils Chr. Stenseth or Huaiyu Tian.

**Peer review information** *Nature Ecology & Evolution* thanks Greg Adler, Jinbao Liao and the other, anonymous, reviewer(s) for their contribution to the peer review of this work. Peer reviewer reports are available.

**Reprints and permissions information** is available at [www.nature.com/reprints](http://www.nature.com/reprints).

**Publisher's note** Springer Nature remains neutral with regard to jurisdictional claims in published maps and institutional affiliations.

Springer Nature or its licensor (e.g. a society or other partner) holds exclusive rights to this article under a publishing agreement with the author(s) or other rightsholder(s); author self-archiving of the accepted manuscript version of this article is solely governed by the terms of such publishing agreement and applicable law.

© The Author(s), under exclusive licence to Springer Nature Limited 2024

### Acknowledgements

We thank the hundreds of CDC staff and local health workers in Shaanxi province who collected successive data from 1980 to 2022. We are also deeply grateful to P. Zheng for her valuable contributions to this paper. This study was supported by the Fundamental Research Funds for the Central Universities (2233300001); National Key Research and Development Program of China (2022YFC2303803); scientific and technological innovation 2030—major project of new generation artificial intelligence (2021ZD0111201); National Natural Science Foundation of China (82073616, 82204160); research on Key Technologies of Plague Prevention and Control in Inner Mongolia Autonomous Region (2021ZD0006); BNU-FGS Global

<sup>1</sup>State Key Laboratory of Remote Sensing Science, Center for Global Change and Public Health, Beijing Research Center for Respiratory Infectious Diseases, Beijing Normal University, Beijing, China. <sup>2</sup>School of National Safety and Emergency Management, National Key Laboratory of Intelligent Tracking and Forecasting for Infectious Diseases, Beijing Normal University, Zhuhai, China. <sup>3</sup>Shaanxi Provincial Centre for Disease Control and Prevention, Xi'an, China. <sup>4</sup>Department of Pathobiology and Population Science, The Royal Veterinary College, London, UK. <sup>5</sup>Department of Ecology and Evolutionary Biology, Princeton University, Princeton, NJ, USA. <sup>6</sup>Division of Sciences, School of Interwoven Arts and Sciences, Krea University, Sri City, India. <sup>7</sup>School of Biodiversity, One Health and Veterinary Medicine, University of Glasgow, Glasgow, UK. <sup>8</sup>Shaanxi Blood Center/Xi'an Blood Center, Xi'an, China. <sup>9</sup>Center for Infectious Disease Dynamics, Department of Biology, Pennsylvania State University, University Park, PA, USA. <sup>10</sup>Institut de Biologie de l'École Normale Supérieure UMR 8197, Eco-Evolutionary Mathematics, École Normale Supérieure, Paris, France. <sup>11</sup>Unité Mixte Internationale 209, Mathematical and Computational Modeling of Complex Systems, Sorbonne Université, Paris, France. <sup>12</sup>State Key Laboratory of Pathogen and Biosecurity, Academy of Military Medical Sciences, Beijing, China. <sup>13</sup>Department of Biology, University of Oxford, Oxford, UK. <sup>14</sup>Centre for Ecological and Evolutionary Synthesis, Department of Biosciences, Faculty of Mathematics and Natural Sciences, University of Oslo, Oslo, Norway. <sup>15</sup>Centre for Pandemics and One-Health Research, Sustainable Health Unit (SUSTAINIT), Faculty of Medicine, University of Oslo, Oslo, Norway. <sup>16</sup>Vanke School of Public Health, Tsinghua University, Beijing, China. <sup>17</sup>These authors contributed equally: Shan Pei, Pengbo Yu, Jayna Raghvani. <sup>18</sup>These authors jointly supervised this work: Ruifu Yang, Oliver G. Pybus, Andrew P. Dobson, Nils Chr. Stenseth, Huaiyu Tian. ✉e-mail: [sxdcy@126.com](mailto:sxdcy@126.com); [n.c.stenseth@ibv.uio.no](mailto:n.c.stenseth@ibv.uio.no); [tianhuaiyu@gmail.com](mailto:tianhuaiyu@gmail.com)

## Reporting Summary

Nature Portfolio wishes to improve the reproducibility of the work that we publish. This form provides structure for consistency and transparency in reporting. For further information on Nature Portfolio policies, see our [Editorial Policies](#) and the [Editorial Policy Checklist](#).

### Statistics

For all statistical analyses, confirm that the following items are present in the figure legend, table legend, main text, or Methods section.

n/a Confirmed

- The exact sample size ( $n$ ) for each experimental group/condition, given as a discrete number and unit of measurement
- A statement on whether measurements were taken from distinct samples or whether the same sample was measured repeatedly
- The statistical test(s) used AND whether they are one- or two-sided  
*Only common tests should be described solely by name; describe more complex techniques in the Methods section.*
- A description of all covariates tested
- A description of any assumptions or corrections, such as tests of normality and adjustment for multiple comparisons
- A full description of the statistical parameters including central tendency (e.g. means) or other basic estimates (e.g. regression coefficient) AND variation (e.g. standard deviation) or associated estimates of uncertainty (e.g. confidence intervals)
- For null hypothesis testing, the test statistic (e.g.  $F$ ,  $t$ ,  $r$ ) with confidence intervals, effect sizes, degrees of freedom and  $P$  value noted  
*Give  $P$  values as exact values whenever suitable.*
- For Bayesian analysis, information on the choice of priors and Markov chain Monte Carlo settings
- For hierarchical and complex designs, identification of the appropriate level for tests and full reporting of outcomes
- Estimates of effect sizes (e.g. Cohen's  $d$ , Pearson's  $r$ ), indicating how they were calculated

*Our web collection on [statistics for biologists](#) contains articles on many of the points above.*

### Software and code

Policy information about [availability of computer code](#)

Data collection

Data analysis

For manuscripts utilizing custom algorithms or software that are central to the research but not yet described in published literature, software must be made available to editors and reviewers. We strongly encourage code deposition in a community repository (e.g. GitHub). See the Nature Portfolio [guidelines for submitting code & software](#) for further information.

## Data

Policy information about [availability of data](#)

All manuscripts must include a [data availability statement](#). This statement should provide the following information, where applicable:

- Accession codes, unique identifiers, or web links for publicly available datasets
- A description of any restrictions on data availability
- For clinical datasets or third party data, please ensure that the statement adheres to our [policy](#)

All data are available in the main text or the supplementary materials. Raw data are not publicly available and are protected due to confidentiality agreements, which were used under license for the current study, but are available upon reasonable request to the corresponding author and with permission from the data provider (Huaiyu Tian). The request will be responded within 2 weeks.

## Research involving human participants, their data, or biological material

Policy information about studies with [human participants or human data](#). See also policy information about [sex, gender \(identity/presentation\), and sexual orientation](#) and [race, ethnicity and racism](#).

Reporting on sex and gender

We don't have related issues.

Reporting on race, ethnicity, or other socially relevant groupings

We don't have related issues.

Population characteristics

We don't have related issues.

Recruitment

We don't have related issues.

Ethics oversight

We don't have related issues.

Note that full information on the approval of the study protocol must also be provided in the manuscript.

## Field-specific reporting

Please select the one below that is the best fit for your research. If you are not sure, read the appropriate sections before making your selection.

Life sciences

Behavioural & social sciences

Ecological, evolutionary & environmental sciences

For a reference copy of the document with all sections, see [nature.com/documents/nr-reporting-summary-flat.pdf](https://www.nature.com/documents/nr-reporting-summary-flat.pdf)

## Ecological, evolutionary & environmental sciences study design

All studies must disclose on these points even when the disclosure is negative.

Study description

Here, we address this knowledge gap by analyzing a 43-year-long monthly dataset (1980-2022) of synanthropic rodents in central China during intensive land use change. We observed a significant increase in landscape mean patch size, coinciding with a significant fluctuation in rodent community composition and a marked decline in rodent diversity; eight of the nine local rodent species experienced near-extirpation. Our analysis reveals these irregular species fluctuations can be attributed to the intensification effect of land consolidation on species competition among rodents, favoring striped field mice, a critical reservoir host of Hantaan virus (HTNV). Consequently, land consolidation has facilitated the proliferation of striped field mice and increased the prevalence of HTNV among them. This study highlights the importance of considering both direct and indirect effects of anthropogenic activities in the management of biodiversity and public health.

Research sample

No sample-size calculation was performed. The sample size were based on the available data.

Sampling strategy

We don't have related issues.

Data collection

Our study area, the Hu region (108.6° E, 34.1° N) in Shanxi province, Central China, is a predominantly agricultural county. Rodent trapping was carried out for three consecutive nights each month at each of the nine trapping sites located on agricultural land near residential areas. At each site, we deployed 100 traps (four parallel trap lines with 25 traps/line and 5-meter spacing between traps). A total of 308,476 trap nights were conducted from 1980-2022, with a minimum of 300 trap nights per month.

Timing and spatial scale

The raw data was a 43-year-long monthly dataset from 1980 to 2022. Our study area, the Hu region (108.6° E, 34.1° N) in Shanxi province, Central China, is a predominantly agricultural county.

Data exclusions

Data were not excluded.

Reproducibility

Randomization

Blinding

Did the study involve field work?  Yes  No

## Field work, collection and transport

Field conditions

Location

Access & import/export

Disturbance

## Reporting for specific materials, systems and methods

We require information from authors about some types of materials, experimental systems and methods used in many studies. Here, indicate whether each material, system or method listed is relevant to your study. If you are not sure if a list item applies to your research, read the appropriate section before selecting a response.

### Materials & experimental systems

n/a  Involved in the study

Antibodies

Eukaryotic cell lines

Palaeontology and archaeology

Animals and other organisms

Clinical data

Dual use research of concern

Plants

### Methods

n/a  Involved in the study

ChIP-seq

Flow cytometry

MRI-based neuroimaging

## Animals and other research organisms

Policy information about [studies involving animals](#); [ARRIVE guidelines](#) recommended for reporting animal research, and [Sex and Gender in Research](#)

Laboratory animals

Wild animals

Reporting on sex

Field-collected samples	All rodents were accessioned to the Shaanxi CDC [84HX001-13HX141], and retained as voucher specimens for each species. Lung tissues were removed from the trapped rodents and stored immediately at $-196^{\circ}\text{C}$ , and then transported to the biosafety level-2 (BSL-2) laboratory of Shaanxi CDC for processing. The frozen lungs were sliced with a cryostat (Leica CM1950) and preserved in a refrigerator at $-80^{\circ}\text{C}$ . Tissues and serum specimens for serological or molecular tests were handled during the various laboratory procedures in class II type A2 biosafety cabinets.
Ethics oversight	The study's protocol was conducted according to the guidelines of animal welfare set by the World Organization for Animal Health, and approved by the institutional ethics committee of the Shaanxi CDC (Permit numbers: 2014-2 and 2013-005). The species captured in this study were not protected wildlife and were not included in the China Species Red List, therefore a permit to collect wildlife was not required from an official wildlife/conservation agency.

Note that full information on the approval of the study protocol must also be provided in the manuscript.

## Plants

Seed stocks	We don't have related issues.
Novel plant genotypes	We don't have related issues.
Authentication	We don't have related issues.